



Swansea University  
Prifysgol Abertawe



## Cronfa - Swansea University Open Access Repository

---

This is an author produced version of a paper published in:

*Climate Dynamics*

Cronfa URL for this paper:

<http://cronfa.swan.ac.uk/Record/cronfa46055>

---

### Paper:

Nagavciuc, V., Ionita, M., Peroiu, A., Popa, I., Loader, N. & McCarroll, D. (2018). Stable oxygen isotopes in Romanian oak tree rings record summer droughts and associated large-scale circulation patterns over Europe. *Climate Dynamics*, 1-12.

<http://dx.doi.org/10.1007/s00382-018-4530-7>

---

This item is brought to you by Swansea University. Any person downloading material is agreeing to abide by the terms of the repository licence. Copies of full text items may be used or reproduced in any format or medium, without prior permission for personal research or study, educational or non-commercial purposes only. The copyright for any work remains with the original author unless otherwise specified. The full-text must not be sold in any format or medium without the formal permission of the copyright holder.

Permission for multiple reproductions should be obtained from the original author.

Authors are personally responsible for adhering to copyright and publisher restrictions when uploading content to the repository.

<http://www.swansea.ac.uk/library/researchsupport/ris-support/>

1 **Stable oxygen isotopes in Romanian oak tree rings record summer droughts and**  
2 **associated large-scale circulation patterns over Europe**

3  
4 Viorica Nagavciuc<sup>1,2,3,4</sup>, Monica Ionita<sup>5</sup>, Aurel Perşoiu<sup>4,6</sup>, Ionel Popa<sup>7</sup>, Neil J. Loader<sup>8</sup>, Danny  
5 McCarroll<sup>8</sup>

6  
7 <sup>1</sup>Faculty of Forestry, Ştefan cel Mare University, Suceava, Romania

8 <sup>2</sup>Institute for Geological and Geochemical Research, Research Centre for Astronomy and Earth Sciences, Hungarian  
9 Academy of Sciences, Budapest, Hungary

10 <sup>3</sup>Departement of Geography, Johannes Gutenberg University, Mainz, Germany

11 <sup>4</sup>Stable Isotope Laboratory, Ştefan cel Mare University, Suceava, Romania

12 <sup>5</sup>Paleoclimate Dynamics Group, Alfred-Wegener-Institute for Polar and Marine Research, Bussestrasse 24,  
13 Bremerhaven, D-27570, Germany

14 <sup>6</sup>Emil Racoviţă Institute of Speleology, Romanian Academy, Cluj-Napoca, Romania

15 <sup>7</sup>National Research and Development Institute for Silviculture Marin Drăcea, Câmpulung Moldovenesc, Romania

16 <sup>8</sup>Department of Geography, College of Science, Swansea University, Singleton Park, Swansea SA2 8PP, UK

17  
18 *Correspondence to:* nagavciuc.viorica@gmail.com

19  
20  
21  
22  
23  
24  
25  
26  
27 **Abstract**

28 We present the first annual oxygen isotope record (1900 – 2016) from the latewood (LW) cellulose  
29 of oak trees (*Quercus robur*) from NW Romania. As expected, the results correlate negatively with  
30 summer relative humidity, sunshine duration and precipitation and positively with summer  
31 maximum temperature. Spatial correlation analysis reveals a clear signal reflecting drought  
32 conditions at a European scale. Interannual variability is influenced by large-scale atmospheric  
33 circulation and by surface temperatures in the North Atlantic Ocean and the Mediterranean Sea.  
34 There is considerable potential to produce long and well-replicated oak tree ring stable isotope  
35 chronologies in Romania which would allow reconstructions of both regional drought and large-  
36 scale circulation variability over southern and central Europe.  
37  
38

39  
40  
41  
42 **Keywords**

43 Oak,  $\delta^{18}\text{O}$ , Relative Humidity, Dendrochronology, Atmospheric circulation  
44  
45

## 1. Introduction

European droughts and heat waves have increased in frequency and intensity in the 21<sup>st</sup> century (van Lanen et al., 2016; Ionita et al., 2017, 2015), leading to increased risks to human health, property and infrastructure. Climate models suggest that rising global temperatures will lead to more frequent and stronger heat waves and summer droughts in the coming century, with southeastern Europe being particularly affected (Spinoni et al. 2015). The triggering mechanisms behind the genesis and dynamics of heat waves are complex (Kingston et al. 2015; Ionita et al. 2017), and existing observational data are insufficient to offer robust explanations. There is thus a need to look for alternative sources to reconstruct hydroclimatic variability on multi-centennial and longer timescales (Jones and Mann 2004; Huber and Gullede 2011; Smerdon and Pollack 2016).

Tree rings are well established archives of paleoclimatic information, with the advantages of length, annual resolution, precise dating and varied geographical distribution (Schweingruber 1996). However, robust reconstructions of past climate based on measures of tree growth, such as ring width, are restricted to areas where growth is strongly limited by a single well-definable climatic controller. Typically this is summer temperature at high altitudes/latitudes (Popa and Kern 2009; Popa and Bouriaud 2013; Nechita et al. 2017) and precipitation or related hydroclimatic variables in very dry environments (Popa and Sidor 2010; Kern et al. 2012; Levanič et al. 2013; Árvai et al. 2018). Measures of tree ring density (Grudd 2008; Khusek et al. 2015), and the related property of blue reflectance (McCarroll et al. 2002; Wilson et al. 2014), can provide even stronger climatic signals, but are limited to conifers. In contrast, the  $^{18}\text{O}/^{16}\text{O}$  ratio in tree rings is not dependent on net growth, but acts as a passive monitor of environmental change (McCarroll and Loader 2004; Leavitt 2010; Gagen et al. 2011; Young et al. 2015), potentially providing paleoclimate information for regions that are not close to an ecological limit (Haupt et al. 2011; Labuhn et al. 2016). The  $\delta^{18}\text{O}$  values in tree ring cellulose depend on the stable isotope composition of the water taken up by roots, evaporative enrichment in the leaves and on biological fractionation and isotopic exchange occurring during photosynthesis and cellulose formation (McCarroll and Loader 2004; Gessler et al. 2013; Treydte et al. 2014). The  $\delta^{18}\text{O}$  values in soil water are directly influenced by those in precipitation, in turn controlled by atmospheric circulation patterns, condensation temperature, precipitation amount and relative humidity (Dansgaard 1964). The dominant control on the enrichment of leaf water in the heavy isotopes is the difference in vapour pressure of leaf air and ambient air, which is controlled by relative humidity (Gessler et al. 2013; Labuhn et al. 2016). Dry and hot climate conditions lead to an enrichment in  $^{18}\text{O}$  due to evaporation, yielding higher  $\delta^{18}\text{O}$  values in tree-ring cellulose (Labuhn et al. 2016). The dominant environmental signals in tree ring oxygen stable isotope ratios are thus the stable isotope

81 composition of precipitation and summer relative humidity (McCarroll and Loader 2004; Labuhn et  
82 al. 2014; Young et al. 2015).

83 In terms of dendrochronological series, Romania has a high potential to develop a well-  
84 replicated oak chronology covering almost the entire Holocene using the wood from the well-  
85 preserved oak forests together with abundant archaeological and sub-fossil oak timbers (Rădoane et  
86 al. 2015; Kern and Popa 2016; Nechita et al. 2017). This region is characterized by limited tree-  
87 ring-based climate reconstructions (Luterbacher et al. 2016), because tree ring widths are poorly  
88 correlated with climate (Nechita and Popa 2012; Nechita 2014). Strong paleoclimate  
89 reconstructions from this part of south-eastern Europe, where Atlantic, Mediterranean and  
90 Scandinavian climatic influences converge, would fill a clear gap in the paleoclimatic data network  
91 of Europe.

92 This study aims to evaluate the potential of oxygen isotopes in oak tree rings from Romania  
93 for producing long records of hydroclimate, including summer drought, and to assess whether the  
94 local variations in stable oxygen isotope ratios are linked to large-scale atmospheric circulation  
95 patterns over Europe.

96

## 97 **2. Data and methods**

### 98 **2.1 Study area and meteorological data**

99 The Nuşfalău sampling site is situated in north-western Romania, (47.19 °N, 22.66 °E, 270  
100 m above sea level, (Figure 1). The local climate is temperate-continental, with mild winters, hot,  
101 dry summers and westerlies dominating the atmospheric circulation. Local meteorological data for  
102 the period 1961–2013 CE are available from the Romanian Meteorological Administration station  
103 Oradea (47.04 °N, 21.91 °E), 60 km west of the study site. The meteorological data includes:  
104 maximum ( $T_{\max}$ ), mean ( $T_{\text{mean}}$ ), minimum ( $T_{\min}$ ) and soil temperature ( $T_{\text{soil}}$ ), sunshine duration (SS),  
105 cloud cover (CC), relative humidity (RH), and precipitation amount (PP). Highest monthly  
106 precipitation amounts occur in June (78.26 mm on average), and the highest maximum temperatures  
107 are recorded in July (27.2 °C on average) and August (27.2 °C on average). Over the 1961–2013  
108 period, the highest precipitation amount was recorded in June 1980 (178.56 mm), and the highest  
109 monthly maximum temperature was recorded in July 2012 (32.07 °C). The lowest relative humidity  
110 occurs throughout the summer months (June – 71.63 % and July – 69.60 %).

111

### 112 **2.2 Gridded climate data**

113 Gridded precipitation amount totals,  $T_{\text{mean}}$  and the self-calibrated Palmer Drought Severity  
114 Index (scPDSI) covering 1901–2014 CE were extracted from the monthly CRU T.S. 4.01 dataset  
115 (Harris et al. 2013), with a spatial resolution of  $0.5^{\circ} \times 0.5^{\circ}$ . To investigate links with Northern

Commented [DM1]: Do July and August have the same mean?

116 Hemisphere atmospheric circulation we used the seasonal means of Geopotential Height at 500 mb  
 117 (Z500), zonal wind (U500) and meridional wind (V500) at 500 mb from the Twentieth Century  
 118 Reanalysis (V2) data set (NCEPv2; Whitaker et al. 2004; Compo et al. 2006, 2011) on a 2°×2° grid,  
 119 for the period 1901–2014 CE. The vertically integrated water vapor transport (WVT) (Peixoto and  
 120 Oort 1992) was calculated through zonal wind (u), meridional wind (v) and specific humidity (q),  
 121 from the same data set. WVT vectors for latitude ( $\phi$ ) and longitude ( $\lambda$ ) are defined as follows:

$$122 \quad \vec{Q}(\lambda, \phi, t) = Q_{\lambda} \vec{i} + Q_{\phi} \vec{j} \quad \text{eq. (1)}$$

123 Where zonal ( $Q_{\lambda}$ ) and meridional ( $Q_{\phi}$ ) components of Q are given by eq. (2):

$$124 \quad Q_{\lambda} = \int_0^{p_0} qu \frac{dp}{g} \quad \text{eq. (2)}$$

$$Q_{\phi} = \int_0^{p_0} qv \frac{dp}{g}$$

125 where q = specific humidity, u = zonal wind, v = meridional wind and p = pressure. The WVT is  
 126 obtained by summation of water transport for all layers located between the Earth's surface and 300  
 127 hPa, above which the specific humidity in the Twentieth Century Reanalysis (V2) model is zero  
 128 (Kalnay et al. 1996; Whitaker et al. 2004; Compo et al. 2006, 2011). For sea surface temperature we  
 129 used the 1°×1° Hadley Centre Sea Ice and Sea Surface Temperature data set—HadISST (Rayner  
 130 2003).

### 131 **2.3 Development of tree-ring chronologies and statistical methods**

132 Two 5 mm increment cores were collected from each of ten oak trees (*Quercus robur* L.) in  
 133 August 2016 at Nuşfalău using standard dendrochronological sampling methods (Schweingruber  
 134 1988). One core per tree was fixed in a wooden support, polished, scanned and ring widths  
 135 measured using the CDendro software, with a precision of 0.01 mm. Cross dating was performed  
 136 and verified using COFECHA software (Holmes 1983). For stable isotope analysis, nine of the  
 137 unmounted cores were manually dissected with a scalpel under magnification and the latewood  
 138 (summer-wood) sections pooled into one sample. The earlywood is excluded, because in *Q. robur*,  
 139 earlywood vessels are formed about 2-3 weeks before bud burst and are completed before full leaf  
 140 expansion (Puchalka et al. 2017). Alpha-cellulose was extracted from latewood samples following  
 141 the method of Boettger et al. (2007) and Loader et al. (1997) and homogenized using a Hielscher  
 142 ultrasonic device (Laumer et al. 2009). For each sample, 0.30-0.35 mg of cellulose were packed in  
 143 silver capsules, freeze-dried and pyrolyzed using a Thermo Scientific Flash High-Temperature  
 144 Elemental Analyzer (HTEA) and isotope ratios were measured on the evolved CO<sub>2</sub> using a Delta V  
 145 Advantage IRMS in the Stable Isotope Laboratory at Swansea University. Every tenth sample was

147 measured three times, the analytical error being less than 0.3 ‰. The results are expressed using the  
148 conventional  $\delta$  (delta) notation in per mil (‰) relative to the Vienna Standard Mean Ocean Water  
149 (VSMOW) standard (Coplen 1994).

150 Linear correlations between  $\delta^{18}\text{O}$  and local monthly and seasonal climate parameters were  
151 explored using the Treeclim R package (R Development Core Team 2010), with confidence  
152 intervals calculated using the bootstrap method. To identify connections with large-scale  
153 atmospheric circulation and North Atlantic Ocean sea surface temperature (SST), we constructed  
154 composite maps of Z500 and SST standardized anomalies for the summer season by selecting the  
155 years when the value of normalized time series of  $\delta^{18}\text{O}$  values was  $>1$  standard deviation (High) and  
156  $<-1$  standard deviation (Low), respectively. These thresholds were chosen as a compromise  
157 between the strength of the climate anomalies linked to  $\delta^{18}\text{O}$  anomalies and the number of maps  
158 that satisfy this criterion. Further analysis has shown that the results are not sensitive to the exact  
159 threshold value used for the composite analysis (not shown). The significance of the composite  
160 maps is based on a standard t-test (confidence level 95 %).

161

### 162 **3. Results and discussions**

#### 163 **3.1 Local climate signal and links to regional patterns**

164 As expected in samples from a temperate-continental region, the  $\delta^{18}\text{O}$  values are  
165 significantly (95% significance level) and positively correlated with local summer (June-July-  
166 August, JJA) sunshine duration ( $r = 0.55$ ) and maximum temperatures ( $r = 0.48$ ) and significantly  
167 negatively correlated with summer cloud cover ( $r = -0.49$ ) and precipitation amount ( $r = -0.51$ ). The  
168 strongest correlation, however, is with the most direct control on oxygen isotope fractionation in the  
169 leaf, which is summer relative humidity ( $r = -0.67$ ). The calibration model passes standard split-  
170 period verification statistics (NCR 2006), including Reduction of Error (RE) and Coefficient of  
171 Efficiency (CE) (Table 1), suggesting that the relationship is temporally stable, and the correlation  
172 is strong enough to justify a variance-scaled reconstruction, so that past extremes are not routinely  
173 underestimated (McCarroll 2015). Given the short meteorological data set, the calibration -  
174 validation approach is supported by the results of a bootstrap approach to verification with 95%  
175 confidence limits.

176 The spatial validity of the relationship between  $\delta^{18}\text{O}$  ratio and summer precipitation, drought  
177 conditions and temperature was also analyzed, over the period 1901–2016. The  $\delta^{18}\text{O}$  values record  
178 both local signals (Figure S1, Table 2) and signals at a European scale. Significant correlations with  
179 summer PP (Figure 3a) extend over a wide area, with negative correlations over the whole of  
180 southern and central Europe and positive correlations over Fennoscandia. A similar dipole-like  
181 structure in the correlation analysis is found for the summer scPDSI index. High  $\delta^{18}\text{O}$  values are

182 associated with drought conditions over the central and the eastern part of Europe and wet  
183 conditions over Fennoscandia. The highest correlations are found over the eastern part of Europe  
184 (Figure 3b). Strong spatial field correlations are found also for summer maximum temperature  
185 (Figure 3c). High values of  $\delta^{18}\text{O}$  are associated with hot summers over the whole of central and  
186 eastern Europe and cold summers over the northern part of Europe. The dipole-like structure  
187 identified in the correlation maps for PP and scPDSI is a well-known feature of summer  
188 hydroclimate at a European scale (Ionita et al. 2012; Ionita 2015). In general droughts and heat  
189 waves over the central and southern part of Europe are accompanied by prolonged wet and cold  
190 periods over the northern part of Europe, as in the summers of 1904, 1921, 1976 and 2015 (Ionita  
191 et al. 2012; Ionita 2015). This can be regarded as an indication that the  $\delta^{18}\text{O}$  in tree rings for our site  
192 location is able to record not just dry/wet periods at a local scale, but is able to record also dry/wet  
193 periods at a European scale.

194 The highest correlation coefficients were found between  $\delta^{18}\text{O}$  values and summer scPDSI  
195 field. As already indicated by the correlation analysis with local climate data (Table 2),  $\delta^{18}\text{O}$  values  
196 are very sensitive to relative humidity and drought conditions. In order to better analyze the  
197 relationship between  $\delta^{18}\text{O}$  and summer drought, a longer scPDSI series was extracted by averaging  
198 the gridded data over the region (20 °E–25 °E, 45 °N–50 °N). The temporal evolution of the  $\delta^{18}\text{O}$   
199 values and the scPDSI index is shown in Figure 4a. The correlation coefficient between the two-  
200 time series is  $r = -0.52$  ( $p < 0.001$ ) and prolonged dry periods (e.g. 1941–1950) are always associated  
201 with high values of  $\delta^{18}\text{O}$ . A striking feature of the  $\delta^{18}\text{O}$  record is that it captures all of the extremely  
202 dry years (1954, 1976, 2003 and 2015), which were characterized by prolonged and extended  
203 droughts at a European scale (Ionita 2015; Spinoni et al. 2015; Ionita et al. 2017). The good  
204 agreement between the  $\delta^{18}\text{O}$  record and the scPDSI time series and the results of the calibration  
205 model (Table 2) thus indicate that  $\delta^{18}\text{O}$  values can be used as a proxy for the occurrence of dry/wet  
206 condition, especially over the eastern part of Europe.

207 To further explore the scPDSI signal in the  $\delta^{18}\text{O}$  chronology, we compare the probability  
208 distribution function of  $\delta^{18}\text{O}$  values for dry (scPDSI < -2) and wet (scPDSI Index > 2) summers  
209 (Figure 4b). The +/-2 threshold was chosen to focus just on the years that are characterized by  
210 extreme droughts. Values between -2 and 2 for the scPDSI index indicate normal conditions, thus  
211 they are excluded from our analysis. The mean  $\delta^{18}\text{O}$  value for the dry years (29.51 ‰) is  
212 significantly higher ( $p < 0.001$ ) than the mean  $\delta^{18}\text{O}$  value corresponding to wet years (28.13 ‰).

213

### 214 3.2 Moisture signal in the $\delta^{18}\text{O}$ values

215 Figure 5 shows the  $\delta^{18}\text{O}$  time series, the seasonal cycle for precipitation and the daily  
216 maximum temperature for the instrumental period 1961–2013. Years recording the highest  $\delta^{18}\text{O}$

217 values ( $> 1$  standard deviation) and the lowest  $\delta^{18}\text{O}$  years ( $\delta^{18}\text{O} < -1$  standard deviation) (Figure 5a)  
218 were selected and used to calculate the seasonal cycle in precipitation (Figure 5b) and the daily  
219 maximum temperature (Figure 5c). The blue lines (Figure 5b) indicate the seasonal cycle for the  
220 years with high precipitation detected by low  $\delta^{18}\text{O}$  values, while red lines show the seasonal cycle  
221 for years with low precipitation as detected by high  $\delta^{18}\text{O}$  values (Table S1). The black lines indicate  
222 the seasonal cycle computed over the period 1971-2000. As it can be inferred from Figure 5b,  
223 wetter conditions than average (blue lines) are detected from May until August for the extreme low  
224  $\delta^{18}\text{O}$  values. In contrast, drier conditions (red lines) are detected from May to October in  
225 relationship with extreme high  $\delta^{18}\text{O}$  values. For the daily maximum temperature (Figure 5c) blue  
226 lines indicate that these years exhibit low daily maximum temperatures from June to August as  
227 detected by low  $\delta^{18}\text{O}$  values. Red lines indicate that warm conditions prevail from May to August  
228 for years with high  $\delta^{18}\text{O}$  values. The seasonal cycle analysis, for the extreme  $\delta^{18}\text{O}$  values, indicates  
229 that there is no shift in the seasonal cycle for the extreme values, but there is a change in the  
230 absolute values of the analyzed variables. For example, the precipitation amount for low  $\delta^{18}\text{O}$   
231 values in May, June, July and August is more than double that recorded during the years with high  
232  $\delta^{18}\text{O}$  values. This verifies that the  $\delta^{18}\text{O}$  in tree rings is able to capture the occurrence of extreme  
233 summers in terms of precipitation amount and temperature.

234

### 235 **3.3 Tree ring oxygen isotope ratios and large-scale atmospheric circulation**

236 The variations in the  $\delta^{18}\text{O}$  values of tree rings have two major drivers: the stable isotope  
237 composition of the water absorbed through the roots and the evaporative enrichment of this water at  
238 the leaf surface (Roden et al. 2000). As the absorbed water is derived ultimately from precipitation,  
239 and its stable isotope composition can be controlled, inter alia, by atmospheric circulation (e.g. Gat,  
240 1996) we hypothesize that  $\delta^{18}\text{O}$  of tree rings will be able to record the prevailing large-scale  
241 atmospheric circulation. In general, persistent dry (wet) conditions are associated with anticyclonic  
242 (cyclonic) circulation in summer, while the sea surface temperature at the moisture source delivered  
243 to NW Romania plays also an important role via the interaction with large-scale climatic or oceanic  
244 variability (Ionita et al. 2012; Schubert et al. 2014; Ionita 2015). To examine the relationship  
245 between  $\delta^{18}\text{O}$  and large-scale atmospheric circulation we constructed composite maps using  
246 summer northern hemisphere geopotential height at 500mb (Z500) and the vertically integrated  
247 water vapor transport (WVT). We focus on those years when the standardized (z-scored)  $\delta^{18}\text{O} > 1$   
248 standard deviation (High) and  $\delta^{18}\text{O} < -1$  standard deviation (Low). The years that were used for the  
249 composite maps are shown in Table S1.

250 Low  $\delta^{18}\text{O}$  values are associated with a Rossby wave train in the Z500 field, characterized by  
251 a low-pressure system over Greenland, followed by a high-pressure system in the central-north



252 Atlantic Ocean, a low-pressure system located over the central part of Europe and a high-pressure  
253 system over Fennoscandia and western Russia (Figure 6a). This Rossby wave structure in the Z500  
254 field enhances the advection of moisture from the Atlantic towards the central and eastern part of  
255 Europe (Figure 6b). The enhanced moisture transport towards Europe is driven by the low-pressure  
256 system centered over Europe. Enhanced moisture advection leads to higher amounts of precipitation  
257 over the central and eastern part of Europe, which in turn will lead to low  $\delta^{18}\text{O}$  values (amount  
258 effect, Dansgaard, 1964). A similar pattern, in the Z500 field, is obtained when we compute the  
259 composite maps associated with wet summers, based on the scPDSI index (Figure S2a). Positive  
260  $\delta^{18}\text{O}$  values are recorded in association with a horse shoe-like block pattern with a low-pressure  
261 system over the central North Atlantic Ocean, a high-pressure system over the central part of  
262 Europe and a low-pressure system over western Russia (Figure 6c). The anomalous Z500 center  
263 over Europe suggest a dominant subsidence and adiabatic warming associated with reduced  
264 cloudiness, heatwaves and reduced precipitation. The horse shoe-like block deflects the Atlantic  
265 storm tracks towards Fennoscandia (Figure 6d). Warm summers and reduced precipitation will lead  
266 to  $\delta^{18}\text{O}$  values (in agreement with the findings from Figure 5), resulting from both the temperature  
267 effect of the stable isotope composition of precipitation and the potential sub-cloud evaporation of  
268 falling raindrops in a dry atmosphere. Strong evaporative enrichment at the leaf surface (as  
269 expected during warm and dry spells) would further enrich the water in  $^{18}\text{O}$  over  $^{16}\text{O}$  and drive  $\delta^{18}\text{O}$   
270 to higher values. Dry summers, as defined by the scPDSI index, are also associated with a similar  
271 horse shoe-like blocking pattern in the Z500 field (Figure S2b). From a long-term perspective, the  
272 Rossby wave-like structure identified in Figure 6c was found to be associated with the occurrence  
273 of heat waves and extremely high summer temperatures over the central and eastern part of Europe  
274 (Ionita et al. 2017). This suggests that the inter-annual variability of our Romanian  $\delta^{18}\text{O}$  record  
275 captures very well the spatial structure of a relatively typical large-scale climatological feature that  
276 produces droughts in the central and eastern part of Europe.

277

### 278 **3.4 Tree ring oxygen isotope ratios and North Atlantic Ocean SST**

279 Previous studies have emphasized the role of the Atlantic Ocean and the Mediterranean Sea  
280 SSTs in driving the occurrence of heat waves and droughts over the European region (Feudale and  
281 Shukla 2011; Ionita et al. 2012, 2017; Kingston et al. 2013; Ionita 2015). Following this line,  
282 significant correlations between  $\delta^{18}\text{O}$  values and North Atlantic Ocean SST (Figure 7a) indicate  
283 possible connections between the moisture availability over the eastern part of Europe and  
284 conditions at remote ocean areas. Positive  $\delta^{18}\text{O}$  values are associated with positive SST anomalies  
285 in the North Atlantic Ocean, in a band stretching from 20 °N to 40 °N, the Mediterranean region  
286 and the Black Sea and negative SST anomalies in the central Atlantic Ocean. A similar SST pattern

287 is found if we compute the correlation maps between the scPDSI index and the North Atlantic SST  
288 (Figure 7b). Overall, the structure of the SST anomalies in Figure 7 resembles the SST anomalies  
289 responsible for the occurrence of extreme drought events over the southern and eastern part of  
290 Europe (e.g. in 2003, 2015) (Van Lanen et al. 2016; Ionita et al. 2017). Ionita et al., (2017) have  
291 recently shown that warm Mediterranean SSTs have preceded and occurred concurrently with dry  
292 summers over most of the central and eastern part of Europe. In some particular years (e.g.  
293 summers of 2003 and 2015), extremely dry and hot summers over the central and eastern part of  
294 Europe, have occurred simultaneously with cold SST anomalies in the central Atlantic Ocean. In  
295 general, the North Atlantic Ocean SSTs anomalies can explain many features of the European  
296 droughts and heatwaves (Feudale and Shukla 2011). Mediterranean SSTs usually have an additional  
297 effect, with warm SST's acting to reduce the baroclinicity over the European region and reinforcing  
298 the blocking circulation. Altogether, when favorable phase conditions are met, both the large-scale  
299 atmospheric circulation and the SST act as a driver and/or precursor for the dry/wet conditions at a  
300 European scale. Overall, SST can modulate the tree ring cellulose  $\delta^{18}\text{O}$  ratios by modulating the  
301 prevailing large-scale circulation and the occurrence of droughts and heatwaves. Thus, the local tree  
302 ring  $\delta^{18}\text{O}$  variability can be explained, at least partially, via the ocean-atmosphere interaction.

303

#### 304 **4. Conclusions**

305 The calibration and verification results demonstrate that  $\delta^{18}\text{O}$  values of the latewood  
306 cellulose of oak trees from Romania are a very good proxy indicator for local summer relative  
307 humidity and could be used to provide a long record of summer droughts. Spatial correlation  
308 analysis reveals that the  $\delta^{18}\text{O}$  values also contain information on atmospheric circulation at a  
309 European scale, characterized by a dipole structure: negative correlations with drought conditions  
310 over the central and the eastern part of Europe and positive correlations with wet conditions over  
311 Fennoscandia. The internal variability of  $\delta^{18}\text{O}$  values relates to large-scale summer atmospheric  
312 circulation, with high  $\delta^{18}\text{O}$  values associated with anticyclonic circulation, drought and heat waves  
313 over the central and eastern part of Europe. There is considerable potential to produce long and  
314 well-replicated oak tree ring stable isotope chronologies in Romania which would allow  
315 reconstructions of both regional drought and large-scale circulation variability over southern and  
316 central Europe.

317

318

319 **Acknowledgments.** The research leading to these results has received funding from EEA Financial Mechanism 2009 -  
320 2014 under the project contract no CLIMFOR18SEE. M. Ionita was funded by the Helmholtz Climate Initiative  
321 REKLIM. NJL and DMcC acknowledge support from the UK NERC NE/P011527/1.

322

323

324 **References**

- 325 Árvai M, Morgós A, Kern Z (2018) Growth-climate relations and the enhancement of drought signals in pedunculate  
326 oak (*Quercus robur* L.) tree-ring chronology in Eastern Hungary. *iForest - Biogeosciences and Forestry* 11:267–  
327 274. doi: 10.3832/ifer2348-011
- 328 Beck W, Sanders TGM, Pofahl U (2013) CLIMTREG: Detecting temporal changes in climate-growth reactions – A  
329 computer program using intra-annual daily and yearly moving time intervals of variable width.  
330 *Dendrochronologia* 31:232–241. doi: <http://dx.doi.org/10.1016/j.dendro.2013.02.003>
- 331 Boettger T, Haupt M, Knller K, et al (2007) Wood Cellulose Preparation Methods and Mass Spectrometric Analyses of  
332  $\delta^{13}C$ ,  $\delta^{18}O$ , and Nonexchangeable  $\delta^2H$  Values in Cellulose, Sugar, and Starch: An Interlaboratory Comparison.  
333 *Analytical Chemistry* 79:4603–4612. doi: 10.1021/ac0700023
- 334 Compo GP, Whitaker JS, Sardeshmukh PD, et al (2011) The Twentieth Century Reanalysis Project. *Quarterly Journal*  
335 *of the Royal Meteorological Society* 137:1–28. doi: 10.1002/qj.776
- 336 Compo GP, Whitaker JS, Sardeshmukh PD (2006) Feasibility of a 100-year reanalysis using only surface pressure data.  
337 *Bulletin of the American Meteorological Society* 87:175–190. doi: 10.1175/BAMS-87-2-175
- 338 Coplen TB (1994) Reporting of stable hydrogen, carbon, and oxygen isotopic abundances. *Pure and Applied Chemistry*  
339 66:273–276. doi: 10.1351/pac199466020273
- 340 Dansgaard W (1964) Stable isotopes in precipitation. *Tellus*. doi: 10.3402/tellusa.v16i4.8993
- 341 Feudale L, Shukla J (2011) Influence of sea surface temperature on the European heat wave of 2003 summer. Part II: a  
342 modeling study. *Climate Dynamics* 36:1705–1715. doi: 10.1007/s00382-010-0789-z
- 343 Gagen MH, Mccarroll D, Loader NJ, Robertson I (2011) Stable isotopes in dendroclimatology: moving beyond  
344 “Potential”
- 345 Gessler A, Brandes E, Keitel C, et al (2013) The oxygen isotope enrichment of leaf-exported assimilates - does it  
346 always reflect lamina leaf water enrichment? *New Phytologist* 200:144–157. doi: 10.1111/nph.12359
- 347 Grudd H (2008) Torneträsk tree-ring width and density AD 500–2004: a test of climatic sensitivity and a new 1500-year  
348 reconstruction of north Fennoscandian summers. *Climate Dynamics* 31:843–857. doi: 10.1007/s00382-007-0358-  
349 2
- 350 Harris I, Jones PD, Osborn TJ, Lister DH (2013) Updated high-resolution grids of monthly climatic observations – the  
351 CRU TS3.10 Dataset. *International Journal of Climatology*. doi: 10.1002/joc.3711
- 352 Haupt M, Weigl M, Grabner M, Boettger T (2011) A 400-year reconstruction of July relative air humidity for the  
353 Vienna region (eastern Austria) based on carbon and oxygen stable isotope ratios in tree-ring latewood cellulose  
354 of oaks (*Quercus petraea* Matt. Liebl.). *Climatic Change* 105:243–262. doi: 10.1007/s10584-010-9862-1
- 355 Huber DG, Gullette J (2011) Extreme Weather and Climate Change Understanding the Link, Managing the Risk.  
356 Science and Impacts Program Center for Climate and Energy Solutions 1–13. doi: 10.1002/hyp.7574
- 357 Ionita M (2015) Interannual summer streamflow variability over Romania and its connection to large-scale atmospheric  
358 circulation. *International Journal of Climatology* 35:4186–4196. doi: 10.1002/joc.4278
- 359 Ionita M, Lohmann G, Rimbu N, et al (2012) Interannual to decadal summer drought variability over Europe and its  
360 relationship to global sea surface temperature. *Climate Dynamics* 38:363–377. doi: 10.1007/s00382-011-1028-y
- 361 Ionita M, Tallaksen LM, Kingston D, et al (2017) The European 2015 drought from a hydrological perspective.  
362 *Hydrology and Earth System Sciences* 21:1397–1419. doi: 10.5194/hess-21-3001-2017
- 363 Jones PD, Mann ME (2004) Climate over past millenia. *Reviews of Geophysics* 42:1–42. doi:  
364 10.1029/2003RG000143.CONTENTENTS
- 365 Kalnay E, Kanamitsu M, Kistler R, et al (1996) NCAR 40-year reanalysis project. *Bull Amer Meteor Soc* 77 SRC-  
366 :437–470
- 367 Kern Z, Patkó M, Kázmér M, et al (2012) Multiple tree-ring proxies ( earlywood width , latewood width and d 13 C )  
368 from. *Quaternary International* 1–11. doi: 10.1016/j.quaint.2012.05.037
- 369 Kern Z, Popa I (2016) Dendrochronological and radiocarbon analyses of subfossil oaks from the foothills.  
370 *Geochronometria* 43:113–120. doi: 10.1515/geochr-2015-0038
- 371 Kingston DG, Fleig AK, Tallaksen LM, Hannah DM (2013) Ocean–Atmosphere Forcing of Summer Streamflow  
372 Drought in Great Britain. *Journal of Hydrometeorology* 14:331–344. doi: 10.1175/JHM-D-11-0100.1
- 373 Kingston DG, Stagge JH, Tallaksen LM, Hannah DM (2015) European-scale drought: Understanding connections  
374 between atmospheric circulation and meteorological drought indices. *Journal of Climate* 28:505–516. doi:  
375 10.1175/JCLI-D-14-00001.1
- 376 Klusek M, Melvin TM, Grabner M (2015) Multi-century long density chronology of living and sub-fossil trees from  
377 Lake Schwarzensee, Austria. *Dendrochronologia* 33:42–53. doi: <http://dx.doi.org/10.1016/j.dendro.2014.11.004>
- 378 Labuhn I, Daux V, Girardclos O, et al (2016) French summer droughts since 1326 CE: A reconstruction based on tree  
379 ring cellulose  $\delta^{18}O$ . *Clim Past* 12:1101–1117. doi: doi:10.5194/cp-12-1101-2016
- 380 Labuhn I, Daux V, Pierre M, et al (2014) Tree age, site and climate controls on tree ring cellulose  $\delta^{18}O$ : A case study  
381 on oak trees from south-western France. *Dendrochronologia* 32:78–89. doi: doi:10.1016/j.dendro.2013.11.001
- 382 Laumer W, Andreu L, Helle G, et al (2009) A novel approach for the homogenization of cellulose to use micro-amounts  
383 for stable isotope analyses. *Rapid Communications in Mass Spectrometry* 23:1934–1940
- 384 Leavitt SW (2010) Tree-ring C–H–O isotope variability and sampling. *Science of The Total Environment* 408:5244–  
385 5253. doi: <http://dx.doi.org/10.1016/j.scitotenv.2010.07.057>
- 386 Levanić T, Popa I, Poljanšek S, Nechita C (2013) A 323-year long reconstruction of drought for SW Romania based on

387 black pine (*Pinus nigra*) tree-ring widths. *International journal of biometeorology* 57:703–714. doi:  
388 10.1007/s00484-012-0596-9

389 Loader NJ, Robertson I, Barker a. C, et al (1997) An improved technique for the batch processing of small wholewood  
390 samples to  $\alpha$ -cellulose. *Chemical Geology* 136:313–317. doi: 10.1016/S0009-2541(96)00133-7

391 Luterbacher J, Werner JP, Smerdon JE, et al (2016) European summer temperatures since Roman times. *Environmental*  
392 *Research Letters* 11:024001. doi: doi:10.1088/1748-9326/11/2/024001

393 McCarroll D (2015) “Study the past, if you would divine the future”: A retrospective on measuring and understanding  
394 Quaternary climate change. *Journal of Quaternary Science* 30:154–187. doi: 10.1002/jqs.2775

395 McCarroll D, Loader NJ (2004) Stable isotopes in tree rings. *Quaternary Science Reviews* 23:771–801. doi:  
396 <http://dx.doi.org/10.1016/j.quascirev.2003.06.017>

397 McCarroll D, Pettigrew E, Luckman A, et al (2002) Blue reflectance provides a surrogate for latewood density of high-  
398 latitude pine tree rings. *Arctic, antarctic, and alpine research* 4:450–453

399 NCR (2006) *Surface temperature reconstructions for the last 2,000 years*. Washington, DC.

400 Nechita C (2014) The dendroclimatic signal in *Quercus robur*. *Analele Universității din Oradea, Facultatea Protecția*  
401 *Mediului XXIII*:509–516

402 Nechita C, Popa I (2012) The relationship between climate and radial growth for the Oak (*Quercus robur* L.) in the  
403 Western Plain of Romania. *Carpathian Journal of Earth and Environmental Sciences* 7:137–144

404 Nechita C, Popa I, Eggertsson Ó (2017) Climate response of oak (*Quercus* spp.), an evidence of a bioclimatic boundary  
405 induced by the Carpathians. *Science of the Total Environment* 599–600:1598–1607. doi:  
406 10.1016/j.scitotenv.2017.05.118

407 Peixoto JP, Oort AH (1992) *Physics of Climate*. Springer, New York, USA

408 Popa I, Bouriaud O (2013) Reconstruction of summer temperatures in Eastern Carpathian Mountains (Rodna Mts,  
409 Romania) back to AD 1460 from tree-rings. *International Journal of Climatology* n/a-n/a. doi: 10.1002/joc.3730

410 Popa I, Kern Z (2009) Long-term summer temperature reconstruction inferred from tree ring records from the Eastern  
411 Carpathians. *Climate Dynamics* 32:1107–1117

412 Popa I, Sidor C (2010) Rețeaua românească de dendrocronologie RODENDRONET 1. Conifere. Editura Silvica

413 Puchałka R, Koprowski M, Gričar J, Przybylak R (2017) Does tree-ring formation follow leaf phenology in  
414 Pedunculate oak (*Quercus robur* L.)? *European Journal of Forest Research* 136:259–268. doi: 10.1007/s10342-  
415 017-1026-7

416 R Development Core Team (2010) *R: A language an environment for statistical computing*

417 Rădoane M, Nechita C, Chiriloaei F, et al (2015) Late Holocene fluvial activity and correlations with dendrochronology  
418 of subfossil trunks: Case studies of northeastern Romania. *Geomorphology* 239:142–159. doi:  
419 10.1016/j.geomorph.2015.02.036

420 Rayner NA (2003) Global analyses of sea surface temperature, sea ice, and night marine air temperature since the late  
421 nineteenth century. *Journal of Geophysical Research* 108:4407. doi: 10.1029/2002JD002670

422 Roden J, Lin G, Ehleringer JR (2000) A mechanistic model for interpretation of hydrogen and oxygen isotope ratios in  
423 tree-ring cellulose. *Geochimica et Cosmochimica Acta* 64:21–35

424 Schubert SD, Wang H, Koster RD, et al (2014) Northern Eurasian heat waves and droughts. *Journal of Climate*  
425 27:3169–3207. doi: 10.1175/JCLI-D-13-00360.1

426 Schweingruber F-H (1996) *Tree Rings and Environment. Dendroecology*. Swiss Federal Institute of Forest, Snow and  
427 Landscape Research WSL/FNP, Birmensdorf

428 Schweingruber FH (1988) *Tree Rings Basics and Applications of Dendrochronology*

429 Smerdon JE, Pollack HN (2016) Reconstructing Earth’s surface temperature over the past 2000 years: the science  
430 behind the headlines. *Wiley Interdisciplinary Reviews: Climate Change* 7:746–771. doi: 10.1002/wcc.418

431 Spinoni J, Lakatos M, Szentimrey T, et al (2015) Heat and cold waves trends in the Carpathian Region from 1961 to  
432 2010. *International Journal of Climatology* 35:4197–4209. doi: 10.1002/joc.4279

433 Treyde K, Boda S, Graf Pannatier E, et al (2014) Seasonal transfer of oxygen isotopes from precipitation and soil to the  
434 tree ring: Source water versus needle water enrichment. *New Phytologist* 202:772–783. doi: 10.1111/nph.12741

435 Van Lanen HAJ, Laaha G, Kingston DG, et al (2016) Hydrology needed to manage droughts: the 2015 European case.  
436 *Hydrological Processes* 30:3097–3104. doi: 10.1002/hyp.10838

437 van Lanen RJ, Groenewoudt BJ, Spek T, Jansma E (2016) Route persistence. Modelling and quantifying historical  
438 route-network stability from the Roman period to early-modern times (AD 100–1600): a case study from the  
439 Netherlands. *Archaeological and Anthropological Sciences*. doi: 10.1007/s12520-016-0431-z

440 Whitaker JS, Compo GP, Wei X, Hamill TM (2004) Reanalysis before radiosondes using ensemble data assimilation.  
441 *Bulletin of the American Meteorological Society* 132:2983–2991. doi: 10.1175/1520-  
442 0493(2004)132<1190:RWRUED>2.0.CO;2

443 Wilson R, Rao R, Rydval M, et al (2014) Blue Intensity for dendroclimatology: The BC blues: A case study from  
444 British Columbia, Canada. *The Holocene* 24:1428–1438. doi: 10.1177/0959683614544051

445 Young GHF, Loader NJ, McCarroll D, et al (2015) Oxygen stable isotope ratios from British oak tree-rings provide a  
446 strong and consistent record of past changes in summer rainfall. *Climate Dynamics* 45:3609–3622. doi:  
447 10.1007/s00382-015-2559-4

448

449

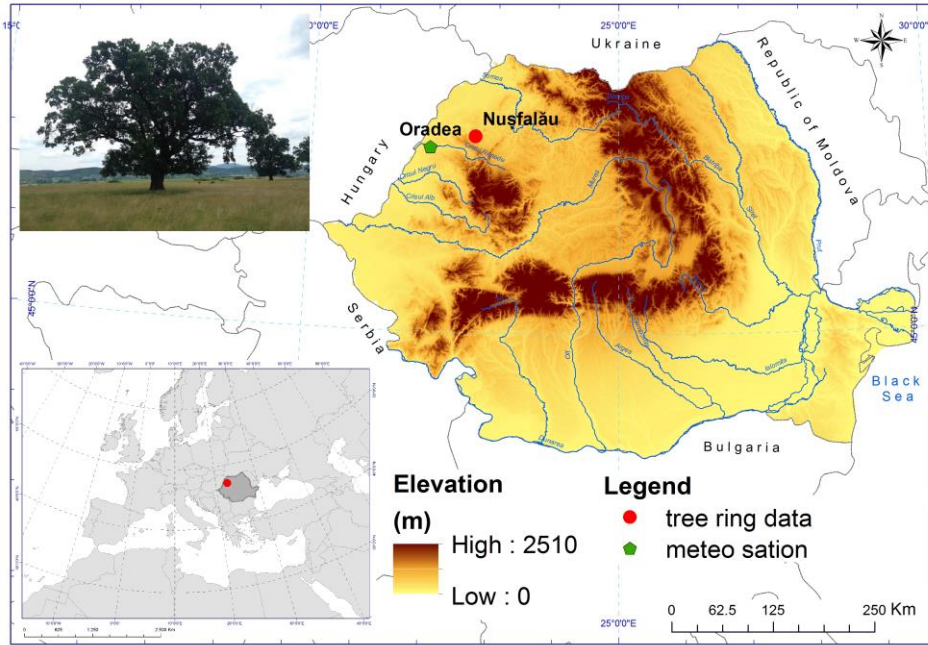
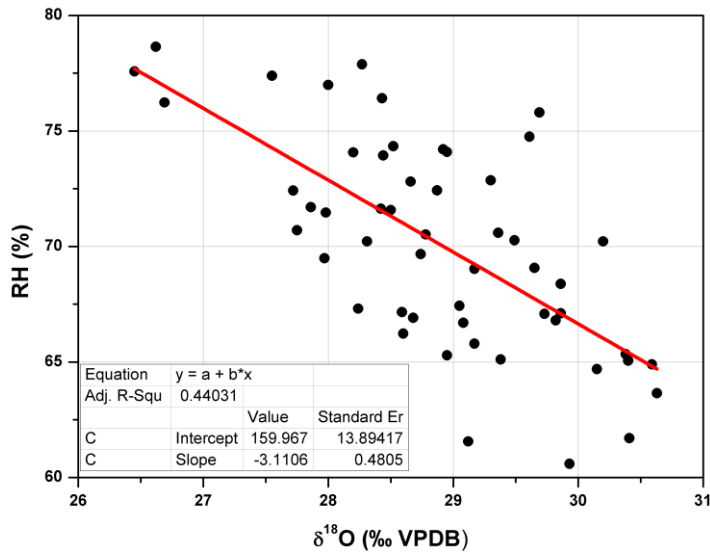


**Figure 1.** Location of the sampling site and the nearby meteorological station (Oradea), and an image of a typical oak tree in this area.

451  
 452  
 453  
 454  
 455  
 456  
 457  
 458  
 459  
 460  
 461  
 462  
 463  
 464  
 465  
 466  
 467  
 468  
 469  
 470  
 471  
 472  
 473  
 474  
 475  
 476  
 477  
 478  
 479

a)



b)

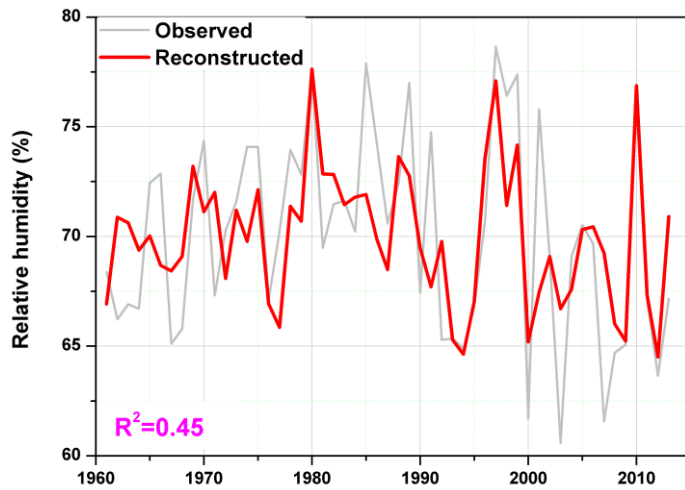


**Figure 2.** a) Regression of summer (JJA) relative humidity on  $\delta^{18}\text{O}$  in the cellulose of late wood (LW) of oak tree-rings and b) Comparison between the observed (gray line) and the reconstruction (red line) mean summer relative humidity over the 1961 – 2013 period.

480  
481  
482  
483  
484  
485  
486  
487  
488  
489  
490

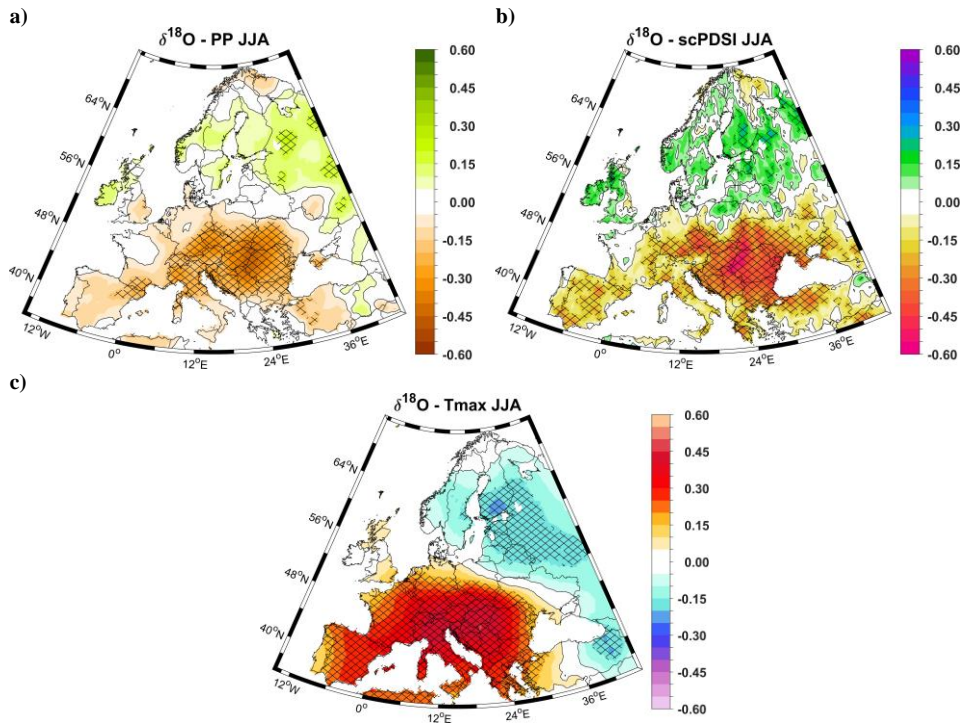


**Figure 3.** a) The spatial correlation map between  $\delta^{18}\text{O}$  and: a) summer precipitation; b) summer scPDSI and c) summer Tmax. The hatching highlights significant correlation coefficients at a confidence level of 95%. Analyzed period: 1901 – 2014.

491  
492  
493  
494  
495  
496  
497  
498  
499  
500  
501  
502  
503  
504  
505  
506  
507  
508  
509  
510  
511  
512  
513  
514  
515  
516  
517

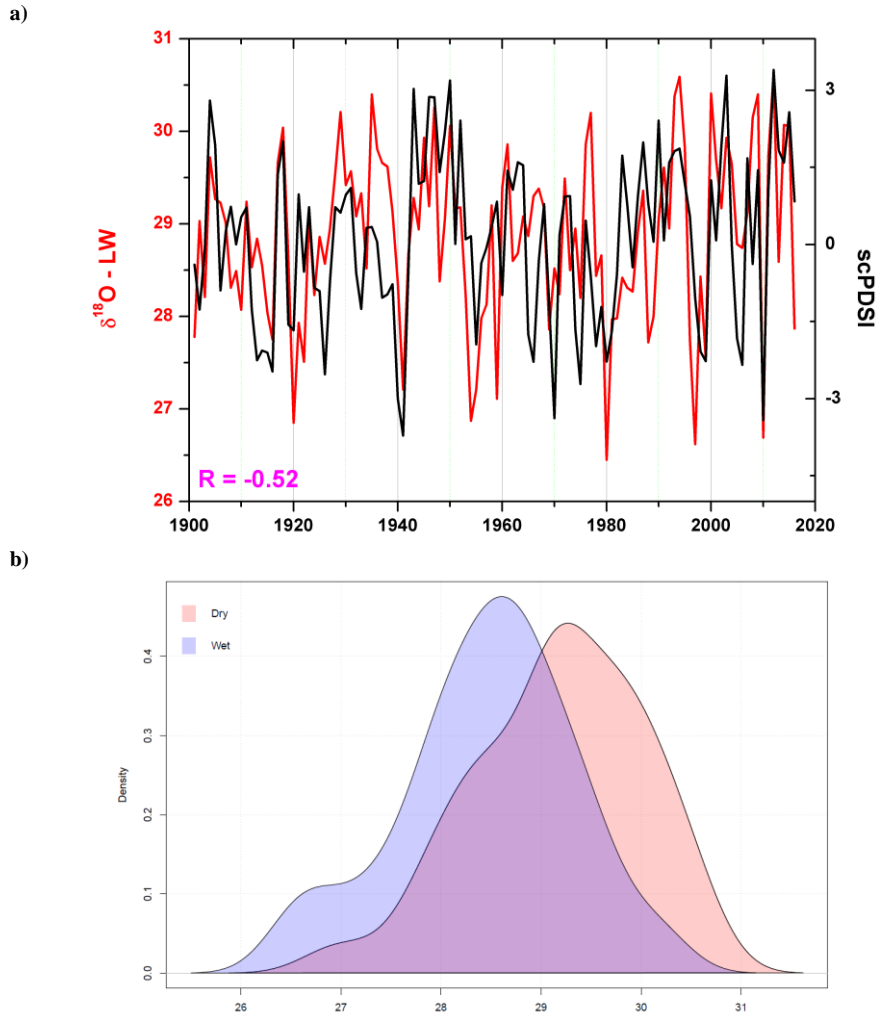
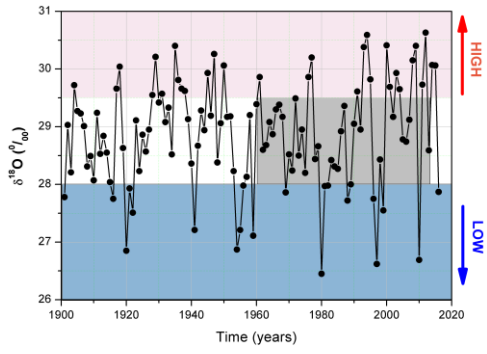


**Figure 4.** a) The temporal evolution of the  $\delta^{18}\text{O}$  (red line) and the scPDSI index (black line) and b) changes in the  $\delta^{18}\text{O}$  probability density function for dry years (scPDSI index  $< -2$ ) and wet years (scPDSI index  $> 2$ ). In a) the scPDSI index was multiplied by  $(-1)$  for a better comparison with the  $\delta^{18}\text{O}$  time series.

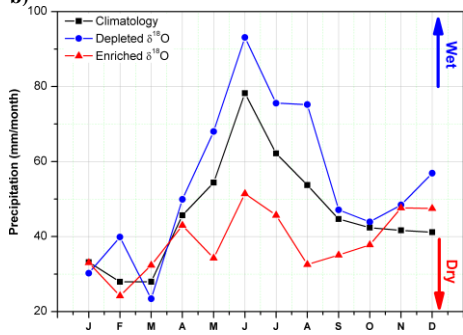
518  
519  
520  
521  
522  
523  
524  
525  
526  
527  
528  
529



a)



b)



c)

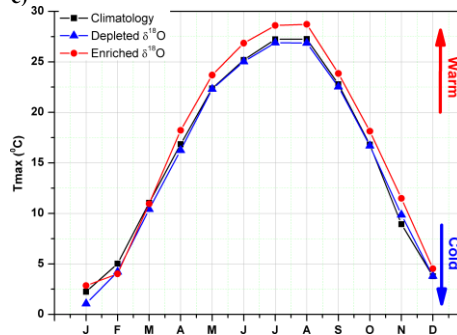
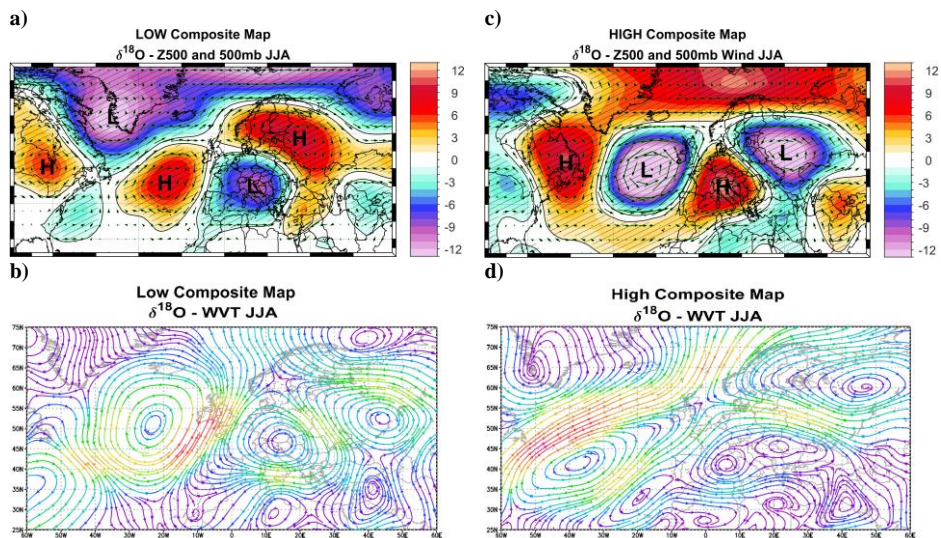


Figure 5. Analyzed period: 1961 – 2013.

530  
531  
532  
533  
534  
535  
536  
537  
538  
539  
540  
541  
542  
543  
544  
545  
546  
547  
548  
549  
550  
551  
552  
553  
554  
555  
556  
557



**Figure 6.** a) The composite map between Low  $\delta^{18}\text{O}$  ( $< -1$  std. dev.) and summer Geopotential Height at 500mb (Z500 – shaded areas) and summer 500mb Wind vectors (arrows); b) the composite map between Low  $\delta^{18}\text{O}$  ( $< -1$  std. dev.) and summer WVT; c) the composite map between High  $\delta^{18}\text{O}$  ( $> 1$  std. dev.) and summer Geopotential Height at 500mb (Z500 – shaded areas) and summer 500mb Wind vectors (arrows) and d) the composite map between High  $\delta^{18}\text{O}$  ( $> 1$  std. dev.) and summer WVT. The years used for the composite maps are shown in Table S1. Analyzed period: 1901 – 2014.

558  
 559  
 560  
 561  
 562  
 563  
 564  
 565  
 566  
 567  
 568  
 569  
 570  
 571  
 572  
 573  
 574  
 575  
 576  
 577  
 578  
 579  
 580  
 581  
 582  
 583  
 584  
 585  
 586  
 587  
 588  
 589

590

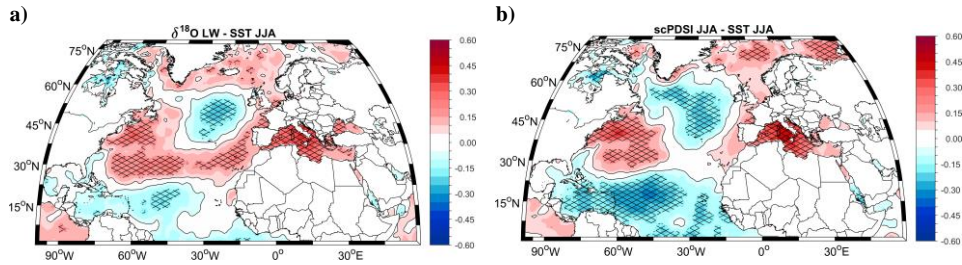


**Figure 7.** a) The correlation map between  $\delta^{18}\text{O}$  LW and JJA SST and b) as in a) but for the summer scPDSI index. The hatching highlights significant correlation coefficients at a confidence level of 95%. Analyzed period: 1901 – 2014.

591  
592  
593  
594  
595  
596  
597  
598  
599  
600  
601  
602  
603  
604  
605  
606  
607  
608  
609  
610  
611  
612  
613  
614  
615  
616  
617  
618  
619  
620  
621  
622  
623  
624  
625  
626  
627  
628  
629  
630

631  
632  
633

**Table 1.** Calibration and verification statistics between  $\delta^{18}\text{O}$  and relative humidity in JJA.

Calibration	Verification	r	R <sup>2</sup>	RE	CE
1961 - 1986		0.49	0.24		
	1986 - 2013	0.73	0.53	0.50	0.45
1987 - 2013		0.73	0.53		
	1961 - 1985	0.51	0.26	0.32	0.16
Full period		0.67	0.45		

634  
635  
636  
637  
638  
639  
640

r = correlation coefficient, R<sup>2</sup> = coefficient of determination, RE = reduction of error, CE = coefficient of efficiency.

**Table 2.** Calibration and verification statistics between  $\delta^{18}\text{O}$  and scPDSI index in JJA.

Calibration	Verification	r	R <sup>2</sup>	RE	CE
1901 - 1958		0.53			
	1959 - 2016	0.52	0.27	0.28	0.26
1959 - 2016		0.52			
	1901 - 1958	0.53	0.28	0.27	0.26
Full period		0.52	0.28		

641  
642

r = correlation coefficient, R<sup>2</sup> = coefficient of determination, RE = reduction of error, CE = coefficient of efficiency.